Bulgarian Chemical Communications, Volume 58, Issue 2 (pp. 173-182) 2026 *DOI: 10.34049/bcc.58.2.5738*

Optimization and performance evaluation of hydroxyapatite–magnesium oxide coatings on UHMWPE for improved tribological and antibacterial behavior in orthopaedic applications

A. Samraj Selvaraj[1]*, A. Sanmugam[1], A. Muniyappan[2]

[1]*Department of Applied Chemistry, Sri Venkateswara College of Engineering, Sriperumbudur, Tamil Nadu, 602117 India*
[2]*Department of Mechanical Engineering, Sri Venkateswara College of Engineering, Sriperumbudur, Tamil Nadu, 602117 India*

Received: December 01, 2025; Revised: April 21, 2026

Ultra-high molecular weight polyethylene (UHMWPE) remains the leading bearing material for joint prostheses, favored for its excellent biocompatibility and mechanical characteristics. However, wear-induced osteolysis remains a significant challenge. This study delves into the development and characterization of hydroxyapatite (HA) and magnesium oxide (MgO) coatings, both singly and in combination, applied to the surface of UHMWPE to enhance its tribological and antibacterial properties. Systematically varied key parameters of the dip-coating process were: immersion speed (IS), dwell time (DT), and withdrawal speed (WS). Through ANOVA analysis, the optimal input conditions for the dip-coating procedure were identified. The performance was subsequently assessed using a pin-on-disc tribometer under dry sliding conditions. This experimental study results indicate that UHMWPE coated with HA-MgO dual layers exhibited a marked reduction in the coefficient of friction (COF) and specific wear rate compared to both uncoated and singly coated UHMWPE samples. Additionally, the antibacterial effectiveness against *Escherichia coli* was significantly enhanced, as evidenced by the larger zones of inhibition on HA-MgO-coated surfaces. These findings highlight the potential of HA-MgO composite coatings to provide multifunctional enhancements for UHMWPE orthopaedic implants, thereby promoting implant longevity and reducing the risk of postoperative infection.

***Keywords*:** Hydroxyapatite, magnesium oxide, dip-coating, pin-on-disc, antibacterial assay, *E. coli* bacteria.

INTRODUCTION

Ultra-high molecular weight polyethylene (UHMWPE) has been integral to orthopaedic implants since the 1960s, primarily due to its high toughness, excellent wear resistance, and biocompatibility. It remains the material of choice for bearing surfaces in total joint arthroplasties, particularly in hip and knee replacements, as evidenced by its dominance in the field [1]. Advances in UHMWPE processing have aimed to mitigate issues such as oxidative degradation and wear particle-induced osteolysis — two major contributors to implant failure. Despite its widespread application, UHMWPE's surface characteristics lead to significant challenges. The effects of γ-ray sterilization and endogenous oxidation can severely diminish its mechanical properties and accelerate wear rates. Oxidized UHMWPE is known to elicit heightened granulocyte activity compared to its unoxidized counterparts, potentially resulting in increased inflammation and expedited implant failure [2]. Furthermore, oxidative processes can induce granulocyte apoptosis, directly affecting the integrity of the implant-tissue interface [3]. The hydrophobic nature of UHMWPE also presents limitations in lubrication by synovial fluid, exacerbating wear issues when compared to the lubrication properties of natural cartilage [4]. To address these challenges, various modifications to both the surface and bulk properties of UHMWPE have been proposed [5]. Crosslinking *via* ionizing radiation enhances durability but can also generate free radicals that contribute to long-term oxidative degradation [6]. The incorporation of vitamin E (α-tocopherol) as an antioxidant has shown promise in mitigating oxidation through diffusion or blending techniques, effectively enhancing oxidative resistance and reducing bacterial adhesion without compromising wear behavior [7]. Moreover, researchers are exploring graftable reactive antioxidants that chemically bond with the polymer matrix during the radiation crosslinking process, thereby improving oxidative stability with minimal additional processing [8]. Surface engineering has emerged as a critical focus, employing methods such as plasma immersion ion implantation and laser surface modification to

* To whom all correspondence should be sent:
E-mail: *allwin.samraj@gmail.com*

enhance wear resistance and biocompatibility through alterations in surface chemistry and microstructure [9, 10]. Ion implantation, in particular, promotes wear resistance by forming nitrogen-carbon crosslinks while preserving the integrity of the surface [11]. Additionally, the combination of ion-implanted UHMWPE with thermally oxidized Ti6Al4V counterfaces has significantly improved tribological performance, enhancing mechanical stability and wear resistance [12]. Porous surface modifications also present opportunities for controlled drug release from acetabular liners, addressing infection prophylaxis while maintaining mechanical integrity — heralding a new era of multifunctional implants [13]. Researchers are exploring surface modifications using bioactive ceramic coatings, specifically hydroxyapatite (HA) and magnesium oxide (MgO), to enhance the bioactivity and osseointegration of ultra-high molecular weight polyethylene (UHMWPE), which exhibits poor integration with bone. Hydroxyapatite, a calcium phosphate analogous to bone mineral, has garnered attention in orthopaedic applications due to its ability to promote cell adhesion and proliferation. Numerous studies indicate that HA coatings on implants significantly enhance osseointegration and osteoconductivity. For example, titanium implants with HA coatings demonstrate improved cell viability and mineralization, particularly when supplemented with natural extracts or dopants [14]. Additionally, dip-coating magnesium alloys with HA not only provides corrosion protection but also maintains cellular compatibility while fostering osteogenesis [15]. Magnesium oxide (MgO), a relatively under-researched bioactive ceramic, shows potential due to its antibacterial properties and ability to modulate cellular responses. When incorporated in HA, magnesium significantly enhances implant performance. Mg-doped HA coatings have been shown to facilitate osseointegration and mechanical fixation in osteoporotic bone models [16] while also mitigating corrosion and inflammatory responses in magnesium alloy substrates [17]. Investigations into HA/Mg composite coatings on stainless steel highlight their superior biocompatibility and bioactivity, particularly when the degradation rate of Mg is controlled to optimize osteogenic outcomes [18]. The synergistic effect of HA and MgO coatings markedly improves both integration and longevity of orthopaedic implants. Composite or bilayer coatings that incorporate HA alongside Mg or MgO not only enhance corrosion resistance and cellular viability but also promote superior bone tissue regeneration compared to single-layer coatings. Research combining HA with magnesium-based polymers has demonstrated that the HA/Mg interface diminishes ion release, slows degradation, and fosters osteoblast proliferation [19]. Notably, double-layer HA coatings with Mg have been found to prevent substrate corrosion and reinforce mechanical strength [20]. Dip-coating has emerged as a cost-effective and efficient technique for applying HA and MgO coatings to orthopaedic materials, ensuring uniform application and strong adhesion. Comparative studies have shown that dip-coating outperforms spin coating in terms of protecting magnesium alloys from corrosion and eliciting cellular responses [21]. Furthermore, dip-coating allows for precise control over coating thickness and uniformity, which minimizes defects such as cracks and delamination [22]. Overall, the application of dip-coated HA and MgO has significant potential for enhancing the longevity and performance of implants by reducing corrosion and wear debris while improving osseointegration. For instance, bioresorbable magnesium implants coated with HA/Mg composites exhibit reduced ion release and enhanced tissue compatibility over time, signaling improved durability and functional efficacy [23].

EXPERIMENTAL

Materials

UHMWPE is a commonly used material in orthopaedic implants, particularly in total joint arthroplasty, due to its excellent wear resistance, low coefficient of friction, biocompatibility, and mechanical toughness. Table 1 presents the material properties of UHMWPE as a biomaterial. In accordance with ASTM G99 standards, the pin specimens were created into cylindrical or spherical shapes from purchased rod material. The specimens were carefully machined to dimensions of 28 mm in length and 10 mm in diameter using wire-cut electrical discharge machining (EDM).

Table 1. Mechanical properties of UHMWPE

Property	Typical value
Density	970 kg/m^3
Tensile strength	20 – 40 MPa
Young's modulus	500 –1500 MPa
Compressive yield strength	38 Mpa
Impact strength	80–160 kJ/m^2 (Izod)
Hardness	Shore D ~62–66
Poisson's ratio	0.33

Figure 1(a) shows the machined UHMWPE pin specimen. The disc serves as the counter body in the setup, while the pin specimens are typically traversed across its surface. For our application involving the interaction of a polymer with metal, a

metal spacer composed of 316L stainless steel is used. This material has a density of 8000 kg/m³, demonstrating favorable mechanical strength along with excellent corrosion resistance. It is a widely used material in biomedical applications, including implants and components for body modification. Figure 1(b) shows an illustration of the disc employed in the pin-on-disc experimental study.

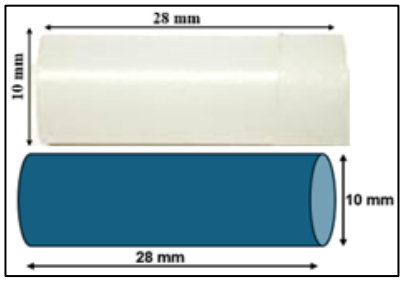

(a)

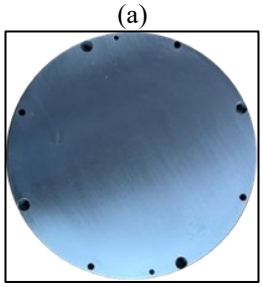

(b)

Figure 1. (a) UHMWPE pin specimen; (b) 316L SS counterpart disc.

Dip-coating process

Hydroxyapatite is typically synthesized *via* wet chemical methods, where calcium nitrate and diammonium hydrogen phosphate are reacted under controlled pH and temperature conditions to precipitate HA particles. These particles are then calcined and suspended in a solvent medium like ethanol or distilled water for coating applications [24]. For MgO, the sol–gel route is commonly used, starting from magnesium alkoxide or nitrate, followed by hydrolysis and drying to form MgO nanoparticles. These are also suspended in a suitable solvent to prepare a stable dip-coating solution [25]. The dip-coating process involves immersing the UHMWPE pins in the prepared suspension of coating material and withdrawing them at a constant speed. This process has been successfully used in several studies to deposit HA and MgO layers on various biomaterials [24, 26]. The following steps are carried out to do the dip-coating process using different coating materials, such as hydroxyapatite and magnesium oxide. First, UHMWPE surfaces are cleaned with ethanol to remove contaminants. The specimen is then immersed in the HA solution at a controlled speed, dipped into the HA solution for a specified dwell time, and withdrawn from the HA solution. After each dip, the specimen is dried at room temperature for up to 60 min to allow solvent evaporation and partial curing [27, 28]. Each specimen typically undergoes five dip cycles per material to achieve optimal surface coverage and adhesion. This repetition builds up a sufficient coating layer while avoiding defects like cracks or peeling [24]. Figure 2 illustrates the dip-coating process for the UHMWPE_HA, UHMWPE_MgO and UHMWPE_HA_MgO specimens. The second coating material, magnesium oxide, is applied in the same manner as the previous steps for HA. Finally, for the composite coatings of hydroxyapatite and magnesium oxide, the order of dipping is critical. Studies recommend coating first with HA to promote osteointegration, followed by MgO to enhance antibacterial and mechanical properties [25, 29]. Table 2 clearly indicates the mass difference after the dip-coating; this increase in mass is due to the coated material added to the substrate.

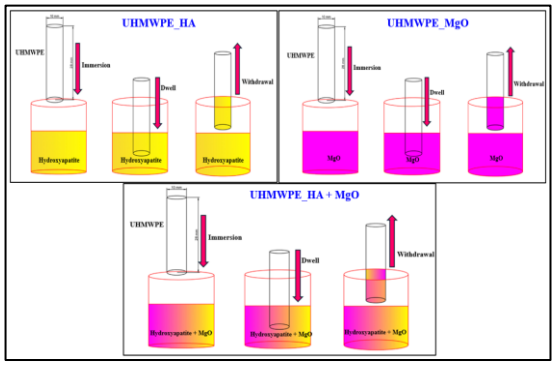

Figure 2. Dip-coating process

Table 2. Mass and hardness values after coating

Specimen type	Mass before coating (g)	Mass after coating (g)	Hardness value HV
UHMWPE	1.963	1.963	7.6
UHMWPE_HA	1.963	2.075	23.5
UHMWPE_MgO	1.960	2.096	25.1
UHMWPE_HA_MgO	1.961	2.135	36.4

Pin-on-disc tribometer

Tribological testing was performed using a pin-on-disc tribometer, shown in Figure 3, following the ASTM G99 standard for wear assessment. In this setup, the pin specimen, oriented vertically, was pressed against a horizontally rotating 316L stainless steel disc. A constant normal load of 100 N was applied throughout the experiment [30], and frictional forces were continuously monitored *via* a load cell. The experimental parameters were standardized to simulate extreme contact conditions relevant to biomedical and engineering applications

employing UHMWPE-based materials, specifically: sliding speed of 2.1 m/s [31], test duration of 10 min, conducted at room temperature under dry sliding conditions.

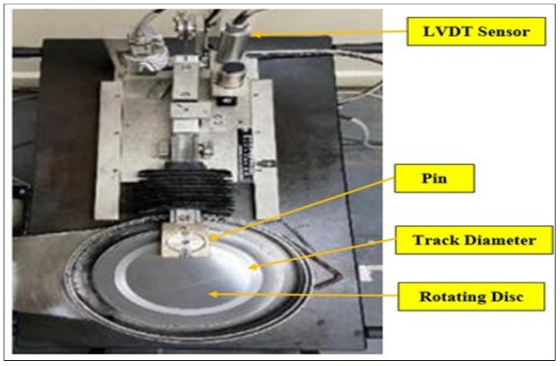

Figure 3. Pin-on-disc tribometer

The specific wear rate of the pin specimens was calculated using the following relations:

$$W = \frac{\Delta V}{F \times L} \quad (1)$$

$$L = v \times t \quad (2)$$

$$\mu = \frac{F_f}{F} \quad (3)$$

where, W - specific wear rate (mm^3/N-m); ΔV - volume loss (mm^3); F - applied normal load (N); L - sliding distance (m); υ - sliding velocity (m/s); t - time period (s); F_f - frictional force.

Table 3 presents the results of the wear test conducted on different UHMWPE-based specimens. It compares the mass of each specimen before and after the wear test, with the corresponding mass loss calculated. Pure UHMWPE showed the highest mass loss (0.201 g), indicating the lowest wear resistance. The incorporation of hydroxyapatite (HA) and magnesium oxide (MgO) significantly reduced the wear loss. Among the composites, UHMWPE reinforced with both HA and MgO exhibited the least mass loss (0.084 g), suggesting that the combined reinforcement enhances wear resistance more effectively than individual fillers.

Table 3. Mass of the specimen before and after the wear test

Specimen type	Mass before wear test (g)	Mass after wear test (g)
UHMWPE	1.963	1.762
UHMWPE_HA	2.071	1.978
UHMWPE_MgO	2.096	2.004
UHMWPE_HA_MgO	2.135	2.054

ANOVA

Table 4. Analysis of variance

Source	DF	SS	MS	F	p-value
Immersion speed	2	0.00165	0.00083	136.34	<0.001
Dwell time	2	0.00040	0.00020	32.67	<0.001
Withdrawal speed	2	0.00044	0.00022	36.43	<0.001
Material	2	0.06758	0.03379	11107.1	<0.001
Immersion × saterial	4	0.00155	0.00039	6.37	<0.001
Dwell × saterial	4	0.00142	0.00036	5.83	<0.001
Withdrawal × saterial	4	0.00038	0.00009	1.48	0.224
Immersion × dwell	4	0.00067	0.00017	2.77	0.038
Immersion × withdrawal	4	0.00007	0.00002	0.27	0.893
Dwell × withdrawal	4	0.00015	0.00004	0.61	0.660
Error	54	0.00033	0.00001	–	–
Total	82	0.07463	–	–	–

Table 4 reveals that immersion speed, dwell time, withdrawal speed, and material type exert statistically significant effects on the response variable ($p < 0.001$ for all factors). Among these, the material exhibits the most dominant influence, with an exceptionally high F-value (11107.1), indicating that the choice of material plays a critical role in governing performance. Immersion speed (F = 136.34), withdrawal speed (F = 36.43), and dwell time (F = 32.67) also contribute significantly, though to a lesser degree. Interaction effects, particularly immersion × material and dwell × material, are also significant ($p < 0.001$), suggesting that the material properties strongly mediate the impact of processing parameters. Conversely, interactions such as withdrawal × material, immersion × withdrawal, and dwell × withdrawal show no significant influence ($p > 0.05$), highlighting that not all parameter combinations are critical. Overall, these results emphasize that optimizing material selection, along with immersion and dwell conditions, is essential for improving system performance, whereas withdrawal-related effects are comparatively less influential.

Antibacterial assay

To evaluate the antibacterial activity of UHMWPE, UHMWPE_HA, UHMWPE_MgO, and UHMWPE_HA_MgO specimens against *E. coli* the zone of inhibition (ZOI) method was used. Figure 4 shows the detailed experimental procedure for the antibacterial assay.

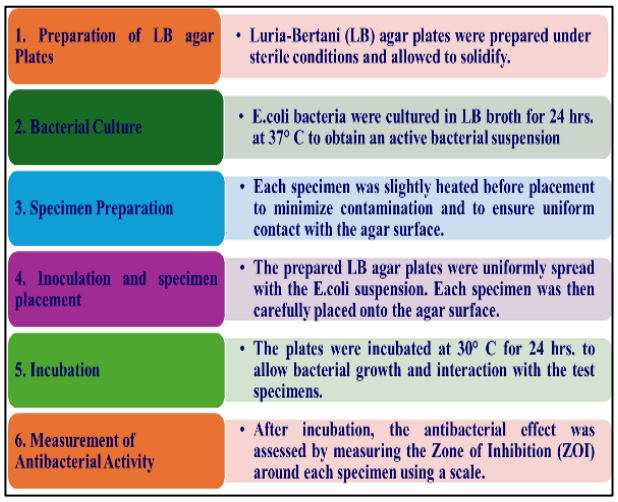

Figure 4. Experimental procedure of antibacterial assay

RESULTS AND DISCUSSION

Main effects of process parameters

Figure 5 shows the main effects plots which demonstrate that immersion speed, dwell time, and withdrawal speed significantly influence both the friction coefficient and the wear rate.

Immersion speed: For both friction coefficient and wear rate, the lowest values were observed at an immersion speed of 7.5 mm/s. At lower speeds (5.0 mm/s), higher friction (0.220) and wear (0.00444 mm³/N-m) were recorded, while further increasing the speed to 10.0 mm/s again elevated both properties. This indicates that moderate immersion speeds promote optimal coating uniformity and adhesion, whereas excessively low or high speeds lead to non-uniform films and poorer tribological performance.

Dwell time: The results show that a dwell time of 30 s consistently minimized friction (0.218) and wear (0.00425 mm³/N-m). Shorter (10 s) and longer (50 s) dwell times resulted in higher values for both responses. This suggests that 30 s is the optimal time window to allow solvent exchange and coating stabilization, whereas insufficient or excessive dwell periods may cause structural instabilities or thickness variations.

Withdrawal speed: Withdrawal speed of 3.5 mm/s yielded the lowest friction (0.218) and wear (0.00428 mm³/N-m), while both slower (2.0 mm/s) and faster (5.0 mm/s) speeds increased these values. This confirms that intermediate withdrawal speeds ensure smooth drainage and film uniformity, while extremes result in uneven coating layers.

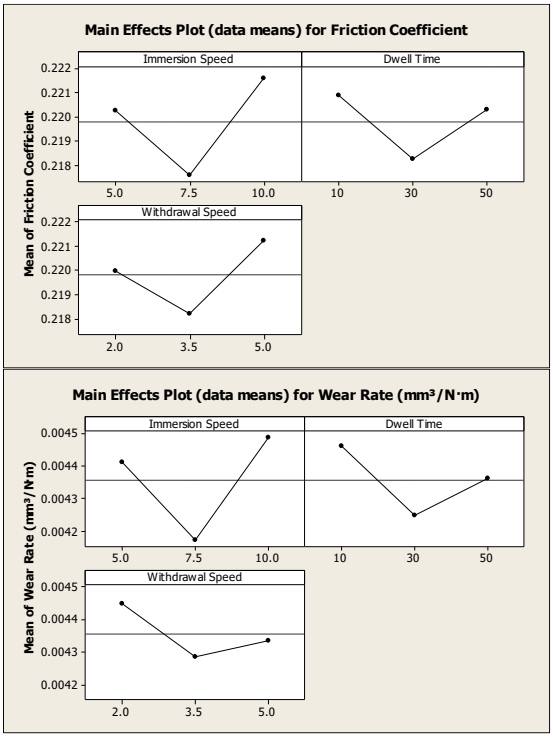

Figure 5. Main effects plot for friction and wear rate

Interaction effects of process parameters

Figure 6 illustrates the interaction plots which provide deeper insights into the coupled effects of the parameters.

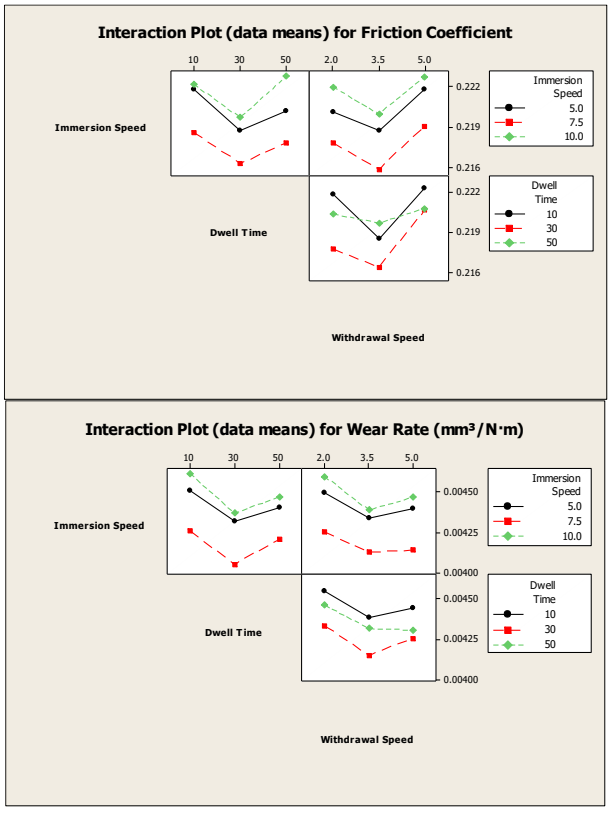

Figure 6. Interaction plot for friction and wear rate

Immersion speed × dwell time: Across immersion speeds, the lowest friction and wear were consistently achieved at a dwell time of 30 s. The benefit of this dwell period was most pronounced at an immersion speed of 7.5 mm/s, highlighting the importance of parameter synergy. At higher immersion speeds (10 mm/s), dwell time had a reduced effect, suggesting less control over coating uniformity.

Withdrawal speed × dwell time: optimal withdrawal speed of 3.5 mm/s and dwell time of 30 s consistently gave the lowest values for both friction and wear. However, at higher withdrawal speeds (5.0 mm/s), differences among dwell times diminished, indicating that excessive withdrawal speed can overshadow the influence of dwell optimization.

Immersion speed × withdrawal speed: For all immersion speeds, the withdrawal speed of 3.5 mm/s resulted in the lowest friction and wear, with the strongest reduction observed at 7.5 mm/s immersion speed. This again confirms the synergistic effect of intermediate immersion and withdrawal rates in producing more stable, uniform coatings.

The results highlight that tribological performance strongly depends on careful optimization of process parameters. Both friction coefficient and wear rate followed similar trends, with intermediate levels of immersion speed, dwell time, and withdrawal speed providing the most favorable outcomes. Mechanistically, these trends may be explained by the dynamics of film formation during dip-coating. At intermediate speeds, the coating layer is more uniform, minimizing asperities that contribute to friction and wear. Likewise, the dwell time of 30 s appears to strike a balance between solvent exchange and coating stabilization, avoiding incomplete deposition at short times and instability at longer times. The optimal combination of parameters is shown in Table 5. This combination consistently produced the lowest friction coefficient (0.218) and wear rate (0.00425 mm³/N-m). Importantly, the alignment of optimal conditions for both properties underscores the robustness of this parameter set in achieving durable, low-friction coatings.

Table 5. Optimum process parameters

Parameter	Optimum value
Immersion speed (IS)	7.5 m/s
Dwell time (DT)	30 s
Withdrawal speed (WS)	3.5 m/s

Effect of process parameters on friction coefficient

Figure 7 shows the variation of the friction coefficient with (a) immersion speed, (b) dwell time, and (c) withdrawal speed for HA, MgO, and HA+MgO coatings. The results show that HA coatings consistently exhibited the highest friction, while HA+MgO coatings achieved the lowest values. In all cases, intermediate processing parameters (7.5 mm/s immersion speed, 30 s dwell time, and 3.5 mm/s withdrawal speed) minimized the friction coefficient, highlighting the importance of parameter optimization for achieving uniform and adherent coatings.

Influence of deposition parameters on wear resistance

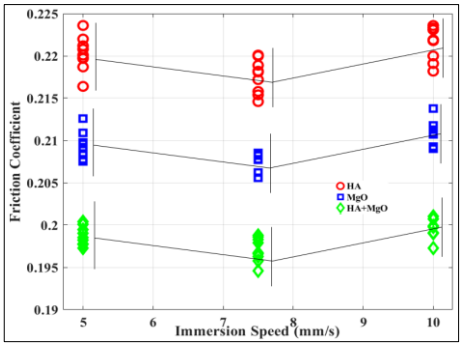

(a)

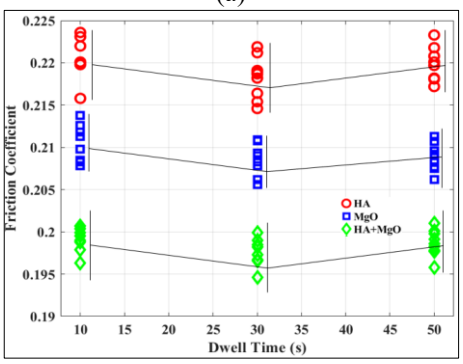

(b)

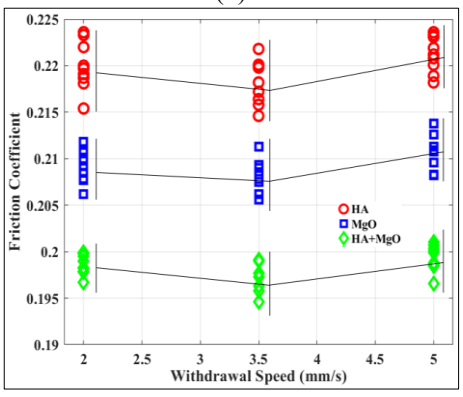

(c)

Figure 7. (a) Friction *versus* immersion speed, (b) Friction *versus* dwell time, (c) Friction *versus* withdrawal speed.

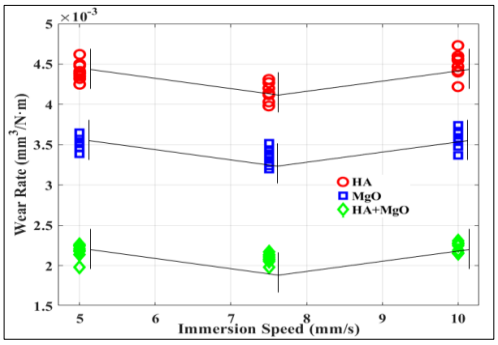

(a)

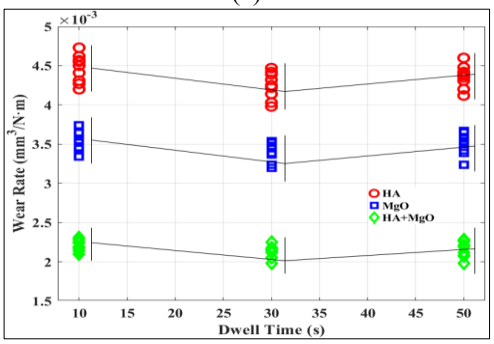

(b)

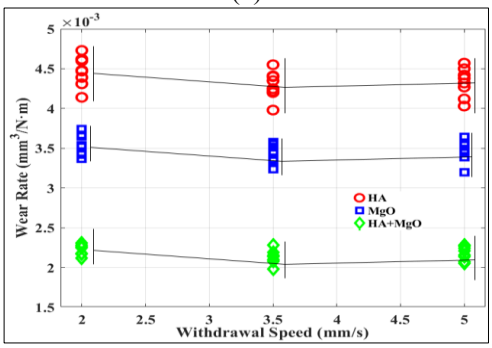

(c)

Figure 8. (a) Wear *versus* immersion speed, (b) Wear *versus* dwell time, (c) Wear *versus* withdrawal speed.

Elemental composition analysis (EDX)

The elemental composition of uncoated UHMWPE and its surface-modified variants was analyzed using energy dispersive X-ray spectroscopy (EDX), with the results illustrated in Figure 9. The EDX spectrum of the base UHMWPE, depicted in Figure 9(a), reveals a predominance of carbon (C) at 92.85 wt.% and oxygen (O) at 5.72 wt.%, characteristic of its polyolefin structure. Minor trace elements detected include titanium (Ti) (0.84 wt.%) and calcium (Ca) (0.59 wt.%), likely originating from environmental interactions or processing residues. Figure 9(b) illustrates the elemental profile of UHMWPE coated with hydroxyapatite (HA), showing substantial alterations in composition. The carbon content diminishes to 32.1 wt.%, whereas oxygen (38.25 wt.%), phosphorus (P, 9.82 wt.%), and calcium (18.4 wt.%) significantly increase, aligning with the hydroxyapatite's composition ($Ca_{10}(PO_4)_6(OH)_2$). This shift confirms the successful deposition of HA onto the UHMWPE surface, with minor peaks of residual sodium (Na) and titanium (Ti) suggesting the influence of processing artefacts. In Figure 9(c), the EDX analysis of the UHMWPE surface coated with magnesium oxide (MgO) reveals a prominent magnesium (Mg) peak at 11.9 wt.%, along with an elevated oxygen content of 25.8 wt.%, indicating effective incorporation of MgO. The carbon content remains substantial (61.5 wt.%) due to the underlying UHMWPE structure, while trace amounts of silicon (Si) and calcium (Ca) may reflect slight cross-contamination or impurities from the synthesis. Figure 9(d) presents the EDX results for the hybrid-coated UHMWPE surface, demonstrating a successful co-deposition of HA and MgO.

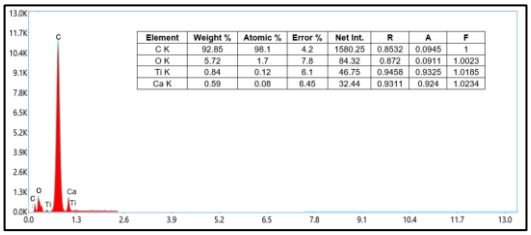

(a)

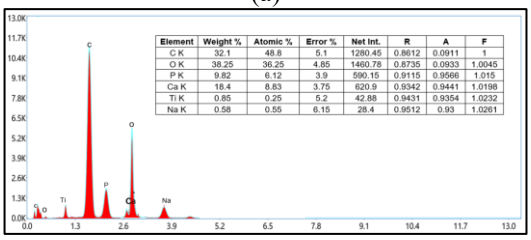

(b)

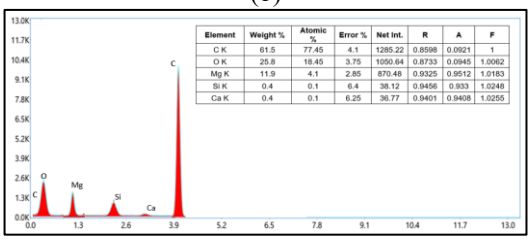

(c)

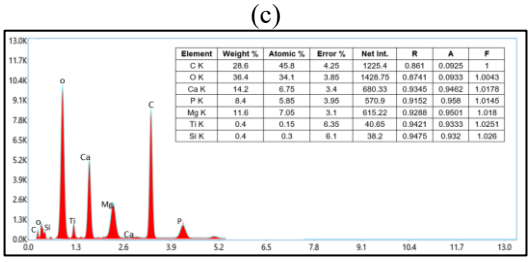

(d)

Figure 9. Element composition of (a) UHMWPE; (b) HA coated; (c) MgO coated; (d) Hybrid coated HA and MgO.

Elemental analysis shows significant levels of oxygen (36.4 wt.%), calcium (14.2 wt.%), magnesium (11.6 wt.%), and phosphorus (8.4 wt.%),

with the carbon content further reduced to 28.6 wt.%, indicative of effective surface coverage. Titanium and silicon are also detected in minor quantities. The EDX findings unequivocally confirm that the surface coatings were successfully deposited on the UHMWPE substrates. The elemental distributions for each sample correspond well with the targeted HA and MgO materials, validating the coating process. The HA-coated surface enhances bioactive elements such as calcium and phosphorus, promoting osteoconductivity and bone integration.

Conversely, the MgO coating introduces magnesium, recognized for its antibacterial properties and its contribution to improved tribological performance through enhanced wear resistance. The synergistic benefits of the dual HA-MgO coating position it as an outstanding candidate for orthopaedic applications, combining bioactivity with antimicrobial functionality.

Tribological behavior of unreinforced UHMWPE and its composites

The tribological behavior of unreinforced UHMWPE and its composites with hydroxyapatite (HA), magnesium oxide (MgO), and hybrid HA–MgO fillers was systematically evaluated in terms of coefficient of friction (COF) and specific wear rate. The variation of COF with sliding distance (Figure 10) shows that unreinforced UHMWPE exhibits the highest and most unstable COF values, fluctuating around 0.23–0.25 throughout the sliding distance. The incorporation of HA slightly reduces the COF (0.21–0.23) while MgO reinforcement demonstrates a more significant improvement, lowering the COF to 0.20. The hybrid composite (UHMWPE_HA_MgO) exhibited the most stable and lowest COF (0.18–0.19), indicating the synergistic effect of HA and MgO in enhancing load-bearing capacity and reducing interfacial shear during sliding.

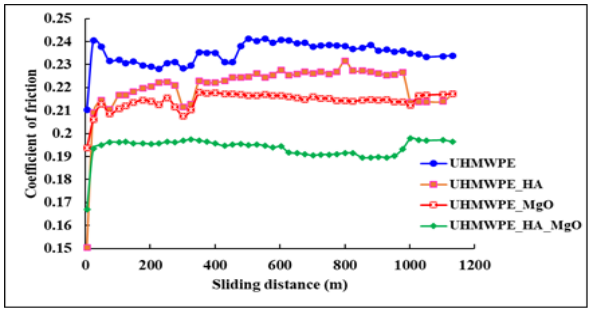

Figure 10. Coefficient of friction *versus* sliding distance

The average COF comparison (Figure 11) further supports this trend, with UHMWPE showing the highest value (0.26), followed by UHMWPE_HA (0.22), UHMWPE_MgO (0.20), and UHMWPE_HA_MgO (0.18). This reduction in COF can be attributed to the improved hardness and load-sharing capability provided by the HA and MgO fillers which reduce polymer chain deformation under load. The hybrid combination likely contributes to improved surface stability by balancing hardness with toughness and dispersion strengthening. At the start of sliding, the contact occurs between fresh, relatively rough asperities of the coating and counterface, leading to higher real contact stress and increased adhesive interaction, which temporarily raises the COF. Additionally, there is no established transfer film or tribolayer at this stage, further contributing to the higher friction value. As the sliding distance increases, surface asperities undergo micro-smoothing and a stable tribolayer (transfer film) forms at the interface. This reduces direct asperity interaction and promotes smoother sliding, resulting in a lower and more stable COF.

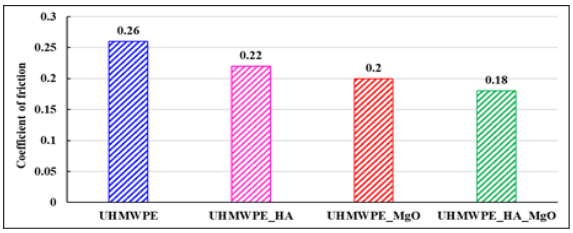

Figure 11. Average coefficient of friction

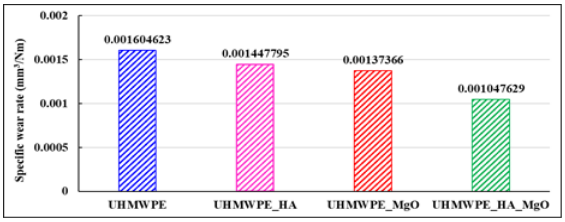

Figure 12. Specific wear rate of UHMWPE and its composite specimens

The specific wear rate analysis (Figure 12) shows a similar trend. Pure UHMWPE has the highest wear rate (1.6046×10^{-3} mm³/Nm), indicating poor resistance to material loss under sliding conditions. The addition of HA decreases the wear rate to 1.4478×10^{-3} mm³/Nm while MgO reinforcement further reduces it to 1.3737×10^{-3} mm³/Nm. The hybrid composite again demonstrates the best performance, with the lowest wear rate of 1.0476×10^{-3} mm³/Nm, representing a 34% improvement compared to pure UHMWPE. This superior wear resistance can be ascribed to improved interfacial bonding and enhanced microstructural stability imparted by the hybrid reinforcement. Overall, the results confirm that reinforcement of UHMWPE with ceramic fillers significantly enhances tribological performance.

While both HA and MgO individually improve friction and wear resistance, the synergistic hybrid reinforcement (HA + MgO) provides the most stable and lowest COF as well as the highest resistance to wear, making UHMWPE_HA_MgO the most promising material among those studied.

Zone of inhibition

Figure 13 shows the antibacterial activity of different UHMWPE composites evaluated using the agar diffusion method against *E. coli* after 24 h of incubation at 30 °C. The results clearly demonstrate that surface modification of UHMWPE with magnesium oxide enhances its antibacterial properties. MgO nanoparticles are known to generate reactive oxygen species and release Mg^{2+} ions, both of which disrupt bacterial cell membranes and inhibit growth.

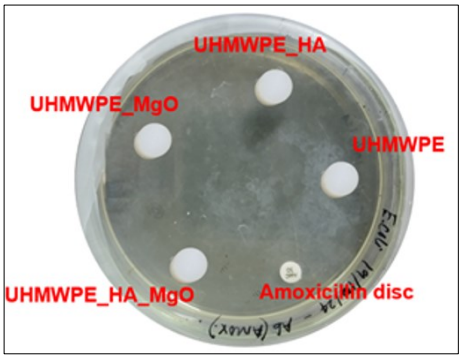

(a)

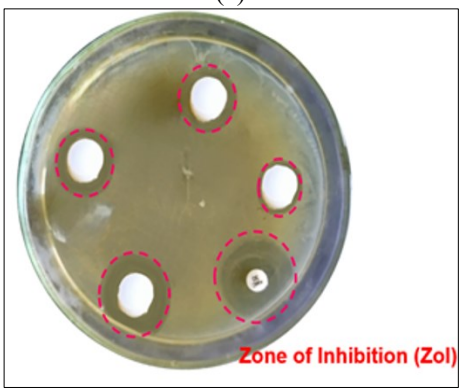

(b)

Figure 13. (a) Before incubation; (b) After 24 h of incubation.

The ZOI observed around UHMWPE_MgO supports this antibacterial mechanism. In contrast, UHMWPE_HA did not exhibit antibacterial activity. Hydroxyapatite is bioactive and osteoconductive, making it useful for bone integration, but it lacks inherent antimicrobial properties. Interestingly, when MgO and HA were combined (UHMWPE_HA_MgO), antibacterial activity was present but appeared weaker compared to MgO alone. This suggests that while HA contributes to biocompatibility, it may reduce the effective surface availability or reactivity of MgO, leading to a smaller ZOI. The unmodified UHMWPE showed no inhibitory effect, which aligns with its known bioinert nature. This confirms that antibacterial enhancement is directly linked to surface modification with MgO. The amoxicillin disc served as a positive control, showing a strong ZOI and validating the bacterial strain's susceptibility to antibiotics. Table 6 shows that magnesium oxide appears to be the key component imparting antibacterial functionality to UHMWPE while hydroxyapatite mainly contributes to bioactivity but does not enhance antimicrobial performance.

Table 6. ZOI for different UHMWPE samples after 24 h at 30 °C

Sample	Zone of inhibition	Antibacterial activity
UHMWPE	None	No activity
UHMWPE_HA	None	No activity
UHMWPE_MgO	Medium	Strong activity
UHMWPE_HA_MgO	Small	Moderate activity
Amoxicillin disc	Large	Very strong activity

Overall, statistical and performance mapping analyses confirmed that coating composition and dwell time were the most influential factors for antibacterial performance, whereas coating composition and intermediate process parameters (immersion and withdrawal speeds) were most significant for tribological enhancement.

CONCLUSION

This study successfully demonstrated that surface modification of UHMWPE using hydroxyapatite (HA), magnesium oxide (MgO), and their hybrid HA–MgO composite *via* dip-coating can significantly enhance the material's functional performance for orthopaedic applications. The experimental results showed that:

(i) *Tribological performance*: The HA–MgO composite coating consistently achieved the lowest coefficient of friction (~0.18–0.19) and the highest wear resistance, representing a ~34% improvement compared to uncoated UHMWPE. This indicates a strong synergistic effect, with HA contributing to hardness and osteoconductivity while MgO improved toughness and load-bearing capacity.

(ii) *Process optimization*: Dip-coating parameters were found to be critical. Intermediate conditions — immersion speed of 7.5 mm/s, dwell time of 30 s, and withdrawal speed of 3.5 mm/s — produced the most uniform coatings, minimizing friction and wear while ensuring coating stability.

(iii) *Antibacterial activity*: MgO was identified as the key contributor to antibacterial functionality, producing strong inhibition against *E. coli*. While HA alone did not exhibit antimicrobial effects, the HA–MgO hybrid provided moderate antibacterial activity alongside improved biocompatibility, suggesting a balanced multifunctional surface.

(iv) *Trade-offs in performance*: Performance maps revealed that while moderate process parameters favored wear and friction reduction, longer dwell times were advantageous for antibacterial performance. The identified compromise — immersion speeds of 7–8 mm/s, withdrawal speeds of 3–4 mm/s, and dwell times of 35–40 s offer a practical balance for maximizing overall implant performance.

In conclusion, the HA–MgO dual-layer coating emerges as the most promising modification strategy, offering superior wear resistance, stable frictional behavior, and enhanced antibacterial protection compared to uncoated or singly coated UHMWPE. These findings highlight the potential of HA–MgO hybrid coatings to extend implant longevity, reduce the risk of postoperative infection, and improve patient outcomes in orthopaedic applications. Future work should explore *in vivo* evaluations and long-term biological responses to validate these multifunctional benefits under physiological conditions.

REFERENCES

1. C. Cucinelli, *Proc. Electr. Insul. Conf. Electr. Manuf. Expo*., 424 (2005).
2. F. Renò, M. Sabbatini, M. Cannas, *J. Mater. Sci.: Mater. Med*., **14**, 241 (2003).
3. F. Renò, F. Lombardi, M. Cannas, *Biomaterials*, **24**, 2895 (2003).
4. S. P. James, R. K. Oldinski, M. Zhang, H. Schwartz, UHMWPE Biomaterials Handbook, 2009, p. 259.
5. S. V. Dorozhkin, *J. Compos. Sci*., **7**, 273 (2023).
6. J. He, Y. Wang, Y. Qian, J. Guo, J. Lu, W. Yang, *Polymers*, **16**, 3431 (2024).
7. P. Bistolfi, G. Bracco, V. Banche, M. Allizond, A. Boffano, E. M. B. Cimino, A. Del Prever, M. Cuffini, *Orthop. Proc*., **96** (B), 83 (2014).
8. S. Jefferies, H. Al-Malaika, H. Sheena, *Polym. Degrad. Stab.*, **183**, 109462 (2021).
9. H. Dong, T. Bell, C. Blawert, B. L. Mordike, *J. Mater. Sci. Lett*., **19**, 1147 (2000).
10. R. Riveiro, J. Soto, R. Del Val, M. Comesaña, F. Boutinguiza, F. Quintero, J. Pou Lusquiños, *Appl. Surf. Sci.*, **302**, 236 (2014).
11. J. Chen, F. Zhu, H. Pan, J. Cao, D. Zhu, H. Xu, Q. Cai, J. Shen, L. Chen, Z. He, *Nucl. Instrum. Methods Phys. Res., Sect. B,* **169**, 26 (2000).
12. W. Shi, H. Dong, *J. Shanghai Univ*. (Engl. Ed.), **9**, 164 (2005).
13. R. Manoj Kumar, P. Gupta, S. K. Sharma, A. Mittal, M. Shekhar, V. Kumar, B. V. Manoj Kumar, P. Roy, D. Lahiri, *Mater. Sci. Eng. C*, **77**, 649 (2017).
14. S. Prabakaran, K. Rohini, *J. Aust. Ceram. Soc*., **61**, 755 (2025).
15. Y. Husak, O. Solodovnyk, A. Yanovska, Y. Kozik, I. Liubchak, V. Ivchenko, O. Mishchenko, Y. Zinchenko, V. Kuznetsov, M. Pogorielov, *Coatings*, **8** (2018).
16. X. Li, Y. Li, Y. Liao, J. Li, L. Zhang, J. Hu, *Int. J. Oral Maxillofac. Implants*, **29**, 196 (2014).
17. M. Razavi, M. Fathi, O. Savabi, D. Vashaee, L. Tayebi, *Mater. Sci. Eng. C,* **48**, 21 (2015).
18. R. Rezaei, B. Golenji, F. Alipour, M. M. Hadavi, I. Mobasherpour, *Ceram. Int*., **46**, 25374 (2020).
19. M. M. Bardizadeh, N. Aboudzadeh, A. Khavandi, A. Eivani, *J. Mater. Res. Technol*., **29**, 2483 (2024).
20. Y. Xu, T. Wang, Y. Guo, G. Li, J. Lian, *Langmuir*, **36**, 13937 (2020).
21. D.-T. Tran, F.-H. Chen, G.-L. Wu, P. C. O. Ching, M.-L. Yeh, *ACS Biomater. Sci. Eng*., **9**, 705 (2023).
22. S. Ardhy Gunawarman, J. Affi, Y. Yetri, *IOP Conf. Ser.: Mater. Sci. Eng*., **1041**, 012057 (2021).
23. R. Rojaee, M. Fathi, K. Raeissi, *Mater. Sci. Eng. C,* **33**, 3817 (2013).
24. V. Morales-Nieto, C. H. Navarro, K. J. Moreno, A. Arizmendi-Morquecho, A. Chávez-Valdez, S. García-Miranda, J. F. Louvier-Hernández, *Prog. Org. Coat*., **76**, 204 (2013).
25. E. Lin, S. S. Kure-Chu, J. Liu, P. Wang, N. Kurita, X. Li, *ECS Meet. Abstr*., **MA2024-02**, 1578 (2024).
26. G. Çelebi Efe, E. Yenilmez, *Surf. Eng*., **38**, 417 (2022).
27. J. Jin, X. Chen, S. Zhou, *Mater. Technol*., **37**, 503 (2022).
28. X. Zhang, X.-W. Li, J.-G. Li, X.-D. Sun, *ACS Appl. Mater. Interfaces*, **6**, 513 (2014).
29. M. L. Dittler, I. Unalan, A. Grünewald, A. M. Beltrán, C. A. Grillo, R. Destch, M. C. Gonzalez, A. R. Boccaccini, *Colloids Surf. B: Biointerfaces*, **182**, 110346 (2019).
30. G. Bergmann, A. Bender, F. Graichen, J. Dymke, A. Rohlmann, A. Trepczynski, M. O. Heller, I. Kutzner, *PLoS One,* **9** (2014).
31. R. Liu, D. Qian, Y. Chen, J. Zou, S. Zheng, B. Bai, Z. Lin, Y. Zhang, Y. Chen, *Sports Biomech*. (2021).